LAWRENCE
LIVERMORE
NATIONAL
LABORATORY

LLNL-JRNL-562854

# Homogeneity of Gd-Based Garnet Transparent Ceramic Scintillators for Gamma Spectroscopy

Z. M. Seeley, N. J. Cherepy, S. A. Payne

June 29, 2012

Journal of Crystal Growth

**Disclaimer**

This document was prepared as an account of work sponsored by an agency of the United States government. Neither the United States government nor Lawrence Livermore National Security, LLC, nor any of their employees makes any warranty, expressed or implied, or assumes any legal liability or responsibility for the accuracy, completeness, or usefulness of any information, apparatus, product, or process disclosed, or represents that its use would not infringe privately owned rights. Reference herein to any specific commercial product, process, or service by trade name, trademark, manufacturer, or otherwise does not necessarily constitute or imply its endorsement, recommendation, or favoring by the United States government or Lawrence Livermore National Security, LLC. The views and opinions of authors expressed herein do not necessarily state or reflect those of the United States government or Lawrence Livermore National Security, LLC, and shall not be used for advertising or product endorsement purposes.

# Homogeneity of Gd-Based Garnet Transparent Ceramic Scintillators for Gamma Spectroscopy

Z. M. Seeley, N. J. Cherepy, S. A. Payne

Chemical Sciences Division

Lawrence Livermore National Laboratory

**Abstract**

Transparent polycrystalline ceramic scintillators based on the composition $Gd_{1.49}Y_{1.49}Ce_{0.02}Ga_{2.2}Al_{2.8}O_{12}$ are being developed for gamma spectroscopy detectors. Scintillator light yield and energy resolution depend on the details of various processing steps, including powder calcination, green body formation, and sintering atmosphere. We have found that gallium sublimation during vacuum sintering creates compositional gradients in the ceramic and can degrade the energy resolution. While sintering in oxygen produces ceramics with uniform composition and little afterglow, light yields are reduced, compared to vacuum sintering. By controlling the atmosphere during the various process steps, we were able to minimize the gallium sublimation, resulting in a more homogeneous composition and improved gamma spectroscopy performance.

Keywords: Transparent ceramic, Garnet, Scintillator, Densification, Sinter-HIP, optical ceramic

## 1. Introduction

Transparent polycrystalline ceramics are fully dense monoliths comprised of small crystallites in random orientations. Usually formed by sintering and densifying ceramic nanoparticles, transparency is achieved by selecting optically isostropic cubic crystal structures and minimizing scattering defects such as residual porosity and the presence of secondary phases. Due to their fabrication via a solid state route, transparent ceramics unveil potential material compositions that would otherwise be difficult to manufacture in the single crystal form due to incongruency and/or high melting points. Optical ceramics are finding use in applications from lasers [1] to armor [2]. Scintillator optics in particular can benefit from the more unusual and complex compositions in order to satisfy the requirements for high stopping, high light yield and fast decay times [3-5]. Ceramics processing also offers a potentially more economic route for fabrication of optics, compared to single crystal growth, as the temperatures utilized are lower, and sintering requires less than a day at temperature, compared to weeks or months for most single crystal growth methods.

Cerium-doped Gadolinium Yttrium Gallium Aluminum Garnet, or GYGAG(Ce) transparent ceramic scintillators are fabricated by producing nanoparticles through a flame spray pyrolysis method, forming them into a green body, which is vacuum sintered, then hot-isostatic pressed into optically transparent parts. We have reported earlier on the gamma spectroscopy performance of transparent ceramic GYGAG(Ce), offering 4.5% resolution at 662 keV with PMT readout and 4% with Silicon

photodiode readout [4]. Offering a principal decay time of 250 ns , an effective atomic number of 47, and density of 5.8 g/cm$^3$, its stopping power is comparable to that of the most commonly used scintillator for gamma spectroscopy, Thallium-doped Sodium Iodide, with $Z_{eff}$ = 50 and density of 3.7 g/cm$^3$. Additionally, GYGAG(Ce) exhibits very low intrinsic radioactivity, high radiation hardness and excellent mechanical and thermal shock toughness.

While we have demonstrated energy resolution of GYGAG(Ce) at 662 keV of 4.5% in small samples, resolution degrades slightly in larger ceramics. Both compositional/material homogeneity and optical light collection homogeneity are critical for high resolution. Material inhomogeneity may result from process conditions that give rise to gradients in stoichiometry and/or Ce-concentration in the ceramic. Optical light collection inhomogeneity, including effects related to self-absorption, as described in Sturm, et al. for Europium-doped Strontium Iodide scintillators [6], can also contribute to resolution degradation in GYGAG(Ce), and its management by optimizing the optical properties of the material and reflector will be addressed in a future paper.

To achieve high material homogeneity, care must be taken during fabrication so as to not create any gradients, especially as the size of the optic increases. Gallium sublimation at high processing temperatures plagues single crystal materials that contain gallium due to large scale gallium gradients [7-10]. We have noticed a similar problem of gallium evaporating from our ceramics; however we report here how this can be avoided by controlling the sintering atmosphere.

**2. Experimental procedure**

Nanoparticles with the composition $Gd_{1.49}Y_{1.49}Ce_{0.02}Ga_{2.2}Al_{2.8}O_{12}$ , GYGAG(Ce),were synthesized via the flame spray pyrolysis (FSP) method by Nanocerox$^{TM}$ (Ann Arbor, MI). A Philips CM300-FEG high resolution transmission electron microscopy (HRTEM) operated at 300 kV was used to characterize the nanoparticles for structure and crystallinity.

Nanoparticles were suspended in an aqueous solution containing polyethylene glycol (PEG) and ammonium polymethacrylate (Darvan C-N) using an ultrasonic probe (Cole Parmer, Vernon Hills, Il) and a high shear mixer (Thinky, Japan). This suspension was poured into a stainless steel mold, sealed to not allow evaporation, and heated to 50°C. Within 24h, the slurry gelled into a solid form and was dried by slowly allowing evaporation. During drying the gel-casting shrank and pulled away from the side walls of the container resulting in a green compact approximately 30% dense [11]. Organics were removed by a heat treatment at 1050°C in air. Calcined compacts were then loaded into a tungsten element vacuum furnace (Thermal Technologies, Santa Rosa, CA) and sintered under a vacuum of $<2\times10^{-6}$ Torr at 1600°C for 2 h to reach closed porosity and densities of approximately 97%. The sintered samples were then hot isostatically pressed (HIP'ed) under 200 MPa of inert argon gas pressure at 1650°C for 4 h in a tungsten element HIP (American Isostatic Presses, Columbus, OH). Since the samples were closed porosity after vacuum sintering, no canning was necessary during the HIP step. Ceramic surfaces were ground and given an inspection polish, and wipe-cleaned with acetone and methanol.

In order to study compositional homogeneities, a JEOL JXA-8200 electron microprobe system was used to measure the composition as a function of location across the fractured surface. Line scans perpendicular to the sample free surface traced inwards 100 µm. Composition was determined by x-ray florescence from cations excited by an electron beam at 20kV and 100 nA.

Pulse height spectra were measured with a $^{137}$Cs source. Samples were optically coupled to a Hamamatsu R6231-100 PMT, which was connected to an Ortec 113 preamplifier, and the signals were shaped with a Tennelec TC 244 spectroscopy amplifier (shaping time of 4 μs) and then recorded with an Amptek MCA8000-A multi-channel analyzer. Spectra were analyzed off-line by non-linear least squares fitting to a Gaussian in order to estimate the energy resolution. Light yields were measured by comparison to a standard YAG(Ce) ceramic from Baikowski.

## 3. Results and discussion

### *3.1 Powder calcination*

As-received powders contain a variety of phases including amorphous, perovskite, and garnet structures as well as some residual organics on the surface leftover from the synthesis process. Powders were calcined between 600 and 1050°C for 1 h. Figure 1 shows TEM images of the as-received and calcined powders. As-received powder contains spherical loosely agglomerated particles with sizes between 20 and 100 nm. The larger particles show some signs of being partly crystallized but the smaller particles appear to be completely amorphous. After calcination at 600°C, the residual organics have been removed, but the particles remain unaffected. By 900°C most particles display some degree of crystallization and some necks between particles indicate the first stages of sintering. After 1050°C, all small particles have sintered together and hard agglomerates are starting to form.

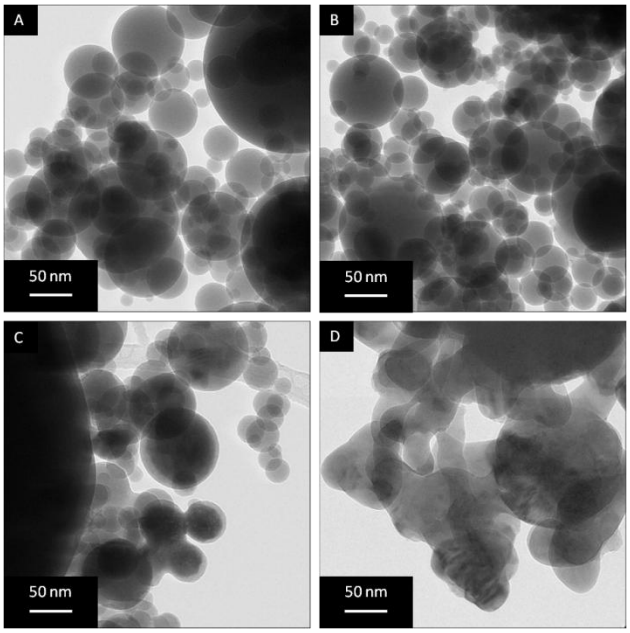


**Fig. 1.** TEM of GYGAG(Ce) powders **(A)** as-received from FSP, and calcined at **(B)** 600°C, **(C)** 900°C, and **(D)** 1050°C.

Powder calcination in air is an important to parameter to optimize prior to fabrication of a green body. We have found that 600°C supplied insufficient crystallization at the powder stage; resulting in additional phase changes and crystallization after the formation of the green body, causing severe cracking. Calcination at 1050°C resulted in large, hard agglomerates hindering the formation of a

uniform density in the green body, and again resulting in the formation of large cracks in the final part. 900°C was identified as the optimal calcination temperature and Figure 2 shows images and microstructures of a cubic inch part at the various stages along the sintering and densification process. After gel-casting, the green body is approximately 30% dense and shows a uniform packing of nanometer-scale particles. During calcination at 1050°C, necks form between all particles and the structure increases in density to about 35%. Vacuum sintering to 1600°C results in significant grain growth to 5 µm, sintering, and densification to approximately 97%. At this stage the monolith is nearly fully dense, however some small micron size pores can still be found by SEM. These pores are isolated from one another (closed porosity) and therefore the parts can be hot isostatic pressed (HIP) at 1650°C without the assistance of canning. After HIP and polishing the monolith is fully dense creating an optic with low optical scatter.

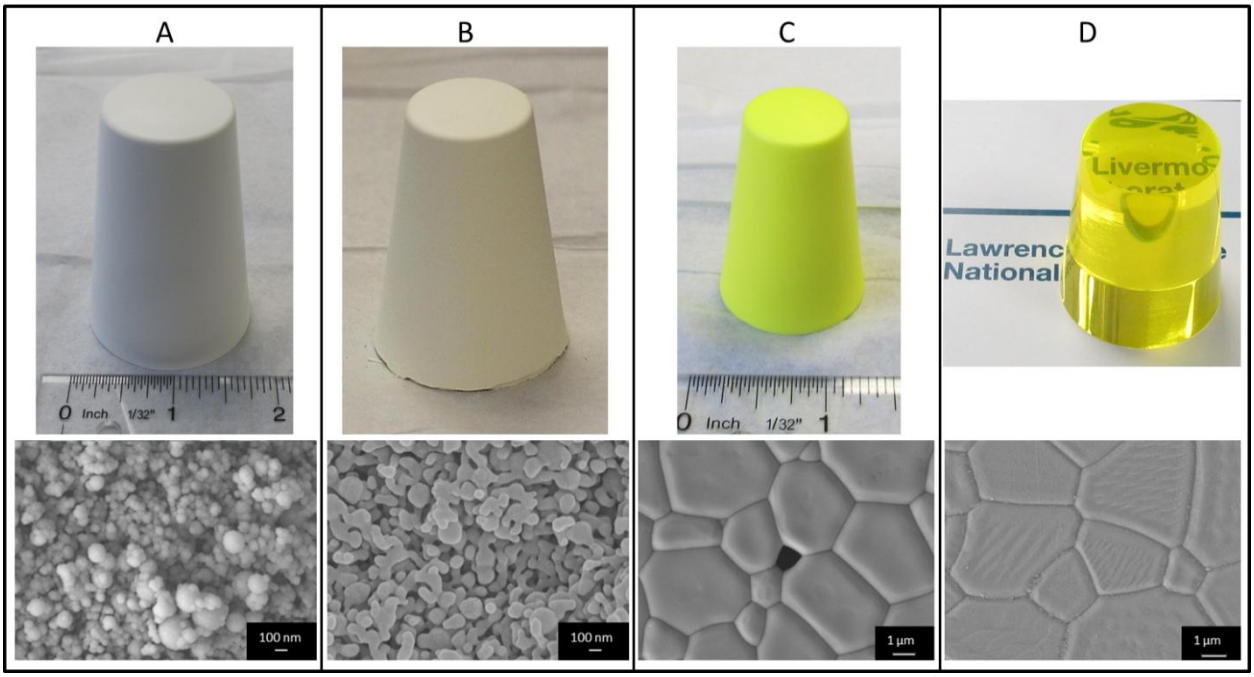


**Fig. 2. (top)** Pictures of **(A)** gel-cast, **(B)** calcined, **(C)** vacuum sintered, and **(D)** HIP'ed. **(bottom)** Microstructure showing the densification process at each step.

*3.2 Sintering atmosphere*

In order to prevent contamination and maximize thermal uniformity during the vacuum sintering step, parts were embedded in coarse $Y_2O_3$ bed powder. This method resulted in sintered parts with a thick white "skin" layer, several microns deep, covering all surfaces of the part which can be seen in Figure 3. An SEM electron probe was used to take compositional line scans from the surface "skin" layer inwards to the bulk of the ceramic. Figure 3 shows the composition of both $Ga_2O_3$ and $Ce_2O_3$ as a function of distance from the surface. These line scans indicate that the white surface "skin" layer on parts embedded in $Y_2O_3$ is severely deficient in gallium. In addition to this depleted layer, there is a gallium gradient that extends up to 100 µm into the bulk of the ceramic. Sublimation of gallium sub-oxide ($Ga_2O$) in a reducing high temperature environment is a common occurrence during the synthesis

of gallium-containing crystals [7-10]. The gallium gradient observed in our ceramics is likely a result of gallium diffusing from high concentration in the bulk to lower concentration in the surface "skin" layer. The compositional line scans also indicated a cerium gradient that appears to be related to the "skin" formation. Figure 3 shows a significant reduction in cerium concentration from bulk to surface, but then the "skin" layer contains the full cerium concentration. Since cerium is a multivalent ion, we might hypothesize that cerium could assist in the formation of gallium sub-oxide and could be transported toward the free surface of the part. However, once this binary system reaches the surface, the gallium sublimes leaving behind the cerium.

To minimize gallium sublimation, we tried sintering our ceramics embedded in coarse GYGAG(Ce) bed powder. As shown in Figure 3, this process resulted in ceramics with virtually no "skin" layer in the surface. In addition, the SEM line scans show that the composition of both gallium and cerium remained constant from the surface to the bulk of the ceramic. Even though the ceramics reduced in size during the sintering cycle and pulled away from the bed powder leaving a void space, it is our hypothesis that the GYGAG(Ce) bed powder created a local partial pressure of gallium surrounding the ceramic minimizing the amount of gallium sublimation from the surface. An alternative route to the formation of ceramics without a depleted "skin" layer is to sinter in an oxidizing environment such as pure oxygen gas or $ZrO_2$ bed powder which releases oxygen at elevated temperatures. Oxygen can diffuse through the oxide matrix even after closed porosity is reached, and we have found that fully dense and transparent ceramics may be created with both of these sintering environments. In the oxygen overpressure method, the gallium never reduces to form the sub-oxide and therefore does not readily sublime [8].

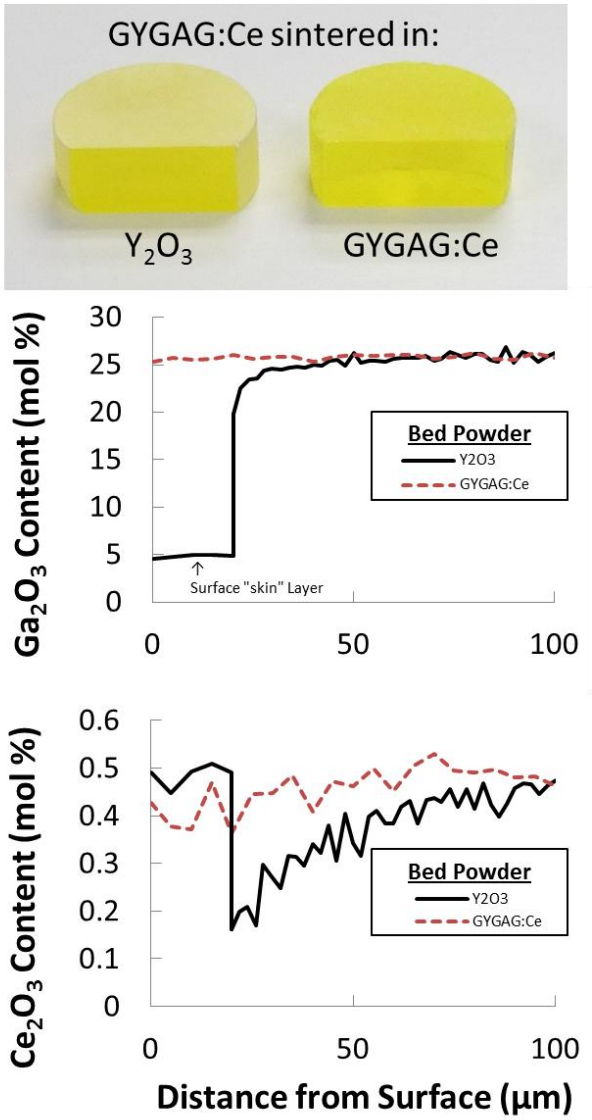


**Fig. 3. (top)** Photograph of GYGAG(Ce) ceramics sintered in $Y_2O_3$ or GYGAG(Ce) bed powder showing white "skin" on part vacuum sintered in $Y_2O_3$ and no skin on part sintered in GYGAG(Ce) bed powder. Electron probe line scans showing compositional gradients of **(middle)** $Ga_2O_3$, and **(bottom)** $Ce_2O_3$ near the surface of ceramics.

Another key aspect involved in the performance of scintillator detectors like GYGAG(Ce) is the defect states present in the final optic. For instance oxygen vacancies are associated with some of the major photoelectron trap states [12]. Trapped photoelectrons release slowly at room temperature causing significant afterglow that lasts up to 24 hours in some of our samples. By altering the environment during ceramic processing we can control the type and concentration of these defects. Figure 4 shows the afterglow 5 seconds after the removal of UV excitation seen by the naked eye for GYGAG(Ce) sintered in vacuum and pure oxygen. It is clearly evident that the ceramics sintered in

vacuum have significantly more afterglow which is likely due to oxygen vacancies formed in the reducing vacuum environment compared with the oxidizing environment.

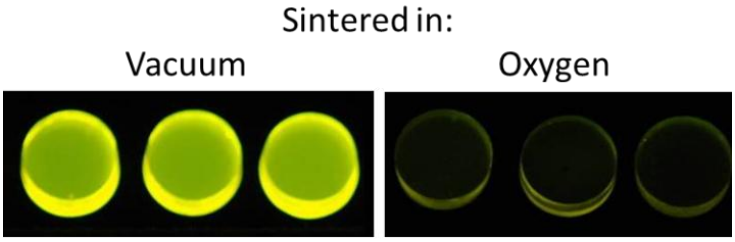


**Fig. 4.** Afterglow approximately 5 seconds after the removal of UV excitation can be seen by the naked eye of GYGAG(Ce) sintered in Vacuum, but not for identical samples sintered in pure oxygen.

*3.3 Scintillation performance as a function of process conditions*

We have found that detector performance, in terms of light yield and energy resolution, for GYGAG(Ce) ceramics is directly related to processing history. Table 1 gives a summary of the various atmospheres and bed powders that were implemented during sintering and the resulting "skin" formation and detector performance. As discussed earlier, vacuum sintering GYGAG(Ce) ceramics in $Y_2O_3$, $Al_2O_3$, or $Gd_2O_3$ bed powder resulted in a gallium depleted "skin" surface layer which caused significant gallium and cerium gradients that extended at least 100 µm into the bulk ceramic. This chemical inhomogeneity changes the scintillation properties even after the surface "skin" layer has been ground off and all surfaces polished. We believe the light yield and energy resolution are degraded where the gallium sublimation occurs due to the related cerium inhomogeneity.

GYGAG(Ce) ceramics sintered in oxygen, or vacuum sintered in $ZrO_2$ bed powder did not form a surface "skin" layer and were more chemically homogeneous, but still provided poorer light yield and worse energy resolution. This phenomenon is attributed to the defects, or lack thereof, created by sintering in an oxygen environment. Ceramics sintered in an oxygen environment are likely to contain fewer oxygen vacancies known to trap photoelectrons. This data suggests that, while oxygen vacancies create long afterglow, the trap states created have a beneficial effect on scintillator light yield. We propose that this is related to the relative trap depth distribution for ceramics processed differently and are in the process of further investigation.

**Table 1.** Formation of surface "Skin" layer, light yield, and energy resolution for GYGAG(Ce) ceramics processed in various sintering conditions.

| Sintering Atmosphere | Bed Powder | "Skin" formation | Light Yield (Ph/ MeV) | Energy resolution (662 keV) |
|---|---|---|---|---|
| Vacuum | $Y_2O_3$ | Yes | 50,000 | 5.26% |
| Vacuum | $Al_2O_3$ | Yes | 51,000 | 5.06% |
| Vacuum | $Gd_2O_3$ | Yes | 48,000 | 5.29% |
| Vacuum | $ZrO_2$ | No | 43,000 | 6.30% |
| Vacuum | GYGAG | No | 55,000 | 4.59% |
| Oxygen | $Y_2O_3$ | No | 44,000 | >9% |

Finally, Figure 5 illustrates the gamma spectrum acquired with a Cs-137 source for the large cubic inch ceramic shown in Fig. 2D and a comparable smaller ceramic. Degradation in energy resolution for the larger ceramic is thought to be due to a combination of material inhomogeneity described previously and optical light trapping, due to the longer average ray length in the large ceramic, resulting in re-absorption by Ce of the scintillation light and red-shifted re-emission that has poorer match to the PMT quantum efficiency. We are in the process of optimizing the chemistry and optic geometry in order to lessen the extent of cerium self-absorption.

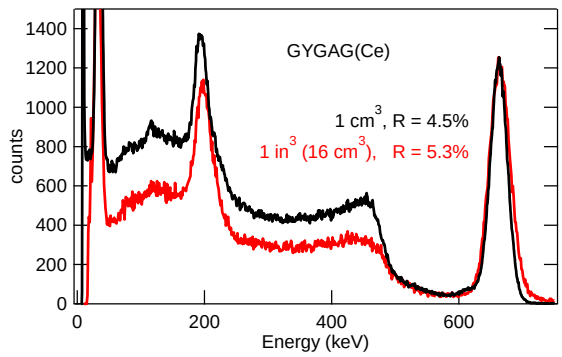


**Fig. 5.** Gamma spectrum acquired with Cs-137 source with 16 $cm^3$ ceramic (Fig. 2D) compared to spectrum obtained with a 1 $cm^3$ GYGAG(Ce) ceramic.

## 4. Conclusions

Cubic inch (16 $cm^3$) scale transparent polycrystalline ceramic optics with the composition $Gd_{1.49}Y_{1.49}Ce_{0.02}Ga_{2.2}Al_{2.8}O_{12}$ (GYGAG(Ce)) were fabricated by the gel-casting method. Calcination of nano-powder is important to start crystallization, however formation of large, hard agglomerates must be avoided. Formation and densification of the green body must be optimized to attain a phase pure ceramic with negligible porosity. Vacuum sintering GYGAG(Ce) in $Y_2O_3$ bed powder caused gallium sublimation from the surface leading to compositional gradients in the ceramic and poor gamma spectroscopy performance. Sintering in an oxygen environment minimized gallium sublimation but changed the oxygen vacancy concentration in the material altering the electron trap state distribution. This greatly reduced the material's afterglow, but also degraded the light yield and energy resolution. The use of coarse GYGAG(Ce) bed powder led to a gallium partial pressure during vacuum sintering and promoted compositional homogeneity while maintaining the correct trap state distribution for good gamma spectroscopy performance.

## Acknowledgments

Thanks to Zurong Dai for electron microscopy, Rick Ryerson for electron probe microscopy, Joshua Kuntz, Keith Lewis and Lindsey Haselhorst with assistance in ceramics fabrication, Sean O'Neal, Owen Drury and Ben Sturm for gamma ray spectroscopy analysis. Thanks to Scott Fisher for mechanical support and Long Nguyen and Todd Stefanik of Nanocerox Inc. for large scale production of nano-

powder. This work has been supported by the US Department of Homeland Security, Domestic Nuclear Detection Office, under competitively awarded IAA HSHQDC-09-x-00208/P00002. This support does not constitute an express or implied endorsement on the part of the Government. LLNL-JRNL-

Prepared by LLNL under Contract DE-AC52-07NA27344.

**References**

1. A. Ikesue, Y-Lin Aung, J. Am. Ceram. Soc., 89 (2006) 1936–1944.

2. J.W. McCauley, P. Patel, M.Chen, G. Gilde, E. Strassburger, B. Paliwal , K.T. Ramesh, D.P. Dandekar, J. European Ceram. Soc., 29 (2009) 223–236.

3. T.Yanagida, H. Takahashi, T. Ito, D. Kasama, T. Enoto, M. Sato, Sh. Hirakuri, M. Kokubun, K. Makishima, T. Yanagitani, H. Yagi, T. Shigeta, T. Ito, IEEE Trans. Nucl. Sci., 52 (2005) 1836.

4. N.J. Cherepy, S.A. Payne, B.W. Sturm, S.P O'Neal, Z.M. Seeley, O.B. Drury, L.K. Haselhorst, B.L. Rupert, R.D. Sanner, P.A. Thelin, S.E. Fisher, R. Hawrami, K.S. Shah, A. Burger, J. O. Ramey, L.A. Boatner, Proc. SPIE, 8142 (2011) 81420W.

5. N.J. Cherepy, S.A. Payne, B.W. Sturm, J.D. Kuntz, Z.M. Seeley, B.L. Rupert, R.D. Sanner, O.B. Drury, T.A. Hurst, S.E. Fisher, M. Groza, L. Matei, A. Burger, R. Hawrami, K.S. Shah, L.A. Boatner, IEEE Nuc. Sci. Symp. Conf. Record, (2010) 1288-1291.

6. B. W. Sturm, N. J. Cherepy, O.B. Drury, P. A. Thelin, S. E. Fisher, S. A. Payne, A. Burger, L. A. Boatner, J. O. Ramey, K. S. Shah, R. Hawrami, Nuc. Inst. Meth. Phys. Res. A 652 (2011) 242-246.

7. D. P. Butt, Y. Park, T. Taylor, J. Nuc. Mater. 264 (1999) 71-77.

8. J. R. Carruthers, M. Kokta, R. L. Barns, M. Grasso, J. Crystal Growth 19 (1973) 204-208.

9. H. Kimura, H. Maeda, M. Sato, J. Crystal Growth 74 (1986) 187-190.

10. K. Kamada, T. Endo, K. Tsutumi, T. Yanagida, Y. Fujimoto, A. Fukabori, A. Yoshikawa, J. Pejchal, and M. Nikl, Cryst. Growth Des. 11 (2011) 4484-4490.

11. J. P. Hollingsworth, J. D. Kuntz, Z. M. Seeley, T. F. Soules, U.S. Patent 8,039,413 B2, Oct. 18, 2011.

12. C. R. Varney, D. T. Mackay, A. Pratt, S. M. Reda, F. A. Selim, J. Appl. Phys. 111 (2012) 063505-063505-7.